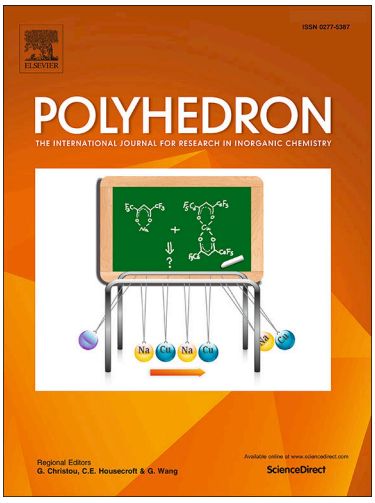

Synthesis and photophysical characterization of novel Ir(III) complexes with a dipyridophenazine analogue (ppdh) as ancillary ligand

Iván González, Josselyn Gómez, Mireya Santander-Nelli, Mirco Natali, Diego Cortés-Arriagada, Paulina Dreyse

PII: S0277-5387(20)30278-3
DOI: https://doi.org/10.1016/j.poly.2020.114621
Reference: POLY 114621

To appear in: *Polyhedron*

Received Date: 29 February 2020
Accepted Date: 27 May 2020

Please cite this article as: I. González, J. Gómez, M. Santander-Nelli, M. Natali, D. Cortés-Arriagada, P. Dreyse, Synthesis and photophysical characterization of novel Ir(III) complexes with a dipyridophenazine analogue (ppdh) as ancillary ligand, *Polyhedron* (2020), doi: https://doi.org/10.1016/j.poly.2020.114621

Synthesis and photophysical characterization of novel Ir(III) complexes with a dipyridophenazine analogue (ppdh) as ancillary ligand

Iván González [a*], *Josselyn Gómez*[b,e], *Mireya Santander-Nelli*[b], *Mirco Natali*[c], *Diego Cortés-Arriagada*[d], *Paulina Dreyse* [b *]

[a]Facultad de Ciencias de la Salud, Universidad Central de Chile, Lord Cochrane 418, Santiago, Chile. e-mail address: ivan.gonzalez@ucentral.cl.

[b]Departamento de Química, Universidad Técnica Federico Santa María, Av. España 1680, Casilla 2390123, Valparaíso, Chile. e-mail address: paulina.dreyse@usm.cl

[c]Department of Chemical and Pharmaceutical Sciences, University of Ferrara, Via L. Borsari 46, 44121 Ferrara, Italy.

[d]Programa Institucional de Fomento a la Investigación, Desarrollo e Innovación. [e]Universidad Tecnológica Metropolitana, Ignacio Valdivieso 2409, P.O. Box 8940577, San Joaquín, Santiago, Chile.

Abstract

Two new complexes $[Ir(ppy)_2ppdh](PF_6)$ (**C1**) and $[Ir(F_2ppy)_2ppdh](PF_6)$ (**C2**), where ppy is 2-phenylpyridine, F_2ppy is 2-(2,4-difluorophenyl)pyridine, and ppdh is pteridino[7,6-f][1,10]phenanthroline-1,13(10H,12H)-dihydroxy have been synthesized. Their photophysical properties have been characterized by means of steady-state and time-resolved emission techniques and supported by TD-DFT calculations. Both complexes **C1** and **C2** are luminescent in fluid solutions at room temperature with quantum yields around ca 1%., and the nature of the emitting excited state has a predominant ^{3}MLCT/^{3}LLCT character with some mixed contributions from a ^{3}LC state on the ancillary ligand. However, in C2 the contribution from the ^{3}LC state becomes dominating, as was identified from a dual emission observed in CH_2Cl_2 arising from a slow equilibration between the ^{3}MLCT/^{3}LLCT and ^{3}LC states. Therefore, the corresponding luminescence is indeed composed of two different patterns (respective maxima at 533 and 580 nm) and two different lifetimes, whose contributions in the whole emission spectrum is strongly dependent on the excitation wavelength. Overall, the results here presented add further fundamental knowledge on the photophysical properties of iridium(III) complexes of potential interest for applications in diverse research fields such as optoelectronics, bioimaging, and theranostics.

Keywords: Iridium complexes; excited state; luminescence; aromatic ligands; dual emission.

Introduction

Transition metal complexes based on Ru(II), Re(I), Pt(II), and Ir(III) have played a leading role in the field of photochemistry and photophysics. These compounds have been used in different applications such as Dye-Sensitized Solar Cells (DSSCs),[1] [2] [3]Organic Light-Emitting Diodes (OLEDs), [4] [5] [6] Light Emitting Electrochemical Cells (LECs), [7] molecular machines, [8] drug delivery[9] [10] [11] and photodynamic therapy (PDT). [12] [13] In all these systems, the design of the metal complex is crucial in order to achieve a specific and controlled light-triggered response.

Cyclometalated Ir(III) complexes have been widely used for the fulfillment of some of these functions due to their versatile structures, attractive photophysical properties, and remarkable stability.[14] [15] [16] In general, the characteristic emission of cyclometalated Ir(III) complexes is phosphorescence ($T_1 \rightarrow S_0$), which is facilitated by the high spin-orbit coupling (SOC) of the metal center. This process typically leads to highly intense luminescence, with energies that can span all the wavelength range of the electromagnetic spectrum according to the electronic nature of the coordinated ligands.[17] Phosphorescent Ir(III) complexes of the general formula $[Ir(C^N)_2(N^N)]^+$, where C^N is the cyclometalating ligand, and N^N is the ancillary ligand, exhibit intense phosphorescence associated to transitions of metal-to-ligand (^{3}MLCT) and ligand-to-ligand (^{3}LLCT) charge transfer character or even of ligand-centered type (^{3}LC), depending on the electronic structures of the ligands. [18] Variation of the C^N or N^N ligands is accomplished to modify the electronic properties of the complexes and, consequently, the respective photophysical behavior.

The dipyrido[3,2-a:2',3'c]phenazine (dppz) ancillary ligand and their complexes have been extensively studied due to their interesting photophysical properties, their relatively simple synthetic procedures, [19] [20] and their biological activities mainly in photodynamic therapy. [21] [22] [23] [24]The structure of dppz ligand is composed of two relevant portions: the phenanthroline (phen) and the phenazine (phz) moieties. Both portions play an important role in the deactivation of the excited state of the complexes, according to the electronic nature of the substituents that these fragments contain. [25] [26] Gordon and co-workers

have used the dppz ligand with appended electron-donor groups in Re(I) complexes, noting that the spectral properties are dominated by strong LC transitions, influenced by the substitutions in the phenazine moiety of the dppz type ligands. [26] Similarly, Jia et al. [27] worked with tetrathiafulvalene substituent on the dppz ligand ((TTF)−dppz) in a series of Ru(II) complexes, where the intramolecular charge transfer states (^{1}ILCT and ^{3}MLCT) were identified as emitters, which is consistent with a dual emission behavior. [27] [28]

Another ligand similar to dppz, is the pteridino[7,6-f][1,10]phenanthroline-1,13(10H,12H)-dione (ppd), which has been synthesized as extended π electron system in order to construct high-performance Ru(II) complexes. This compound shows an absorption band between 350-400 nm assigned to LC of ppd, and other absorption bands between 400-500 nm that corresponds to MLCT transitions. The complex shows a luminescence characteristic of Ru emitters with a maximum peak at ca. 610 nm, as expected for MLCT emitting state of this type of complexes. [29] In other studies, Ji et al. used this ruthenium compound to study its interaction with DNA, finding a high sensitivity for double-strand DNA. However, in spite of these interesting results, no rigorous study of the photophysical properties of these complexes was performed. [30] [31]

Hence, considering that the optical properties of analogous metal complexes with ppd ligands have been sparsely studied, also taking into account their simple synthetic procedures and the different potential applications due to the interesting electronic properties of these type of compound, in this work we synthesized new Ir(III) complexes (Fig. 1) using ppd in its tautomeric form pteridino[7,6-f][1,10]phenanthroline-1,13(10H,12H)-dihydroxy (ppdh), described as $[Ir(ppy)_2ppdh](PF_6)$ (**C1**) and $[Ir(F_2ppy)_2ppdh](PF_6)$ (**C2**), where ppy: 2-phenylpyridine and F_2ppy: 2-(2,4-difluorophenyl)pyridine. Through NMR spectroscopy study, we demonstrate that the tautomer isomer ligand presents hydroxy groups. The ground-state properties of the synthesized Ir(III) complexes were characterized by cyclic voltammetry and absorption spectroscopy, while their photophysical behavior was investigated by steady-state and time-resolved emission techniques. The experimental results have been further supported by TD-DFT calculations. The data obtained show that the decay of the excited states of such metal complexes is

determined by an interplay between excited states of different nature, namely of charge transfer and ligand-centered type. This study will help to develop efficient systems that use the energy of the excited states towards new and diverse applications.

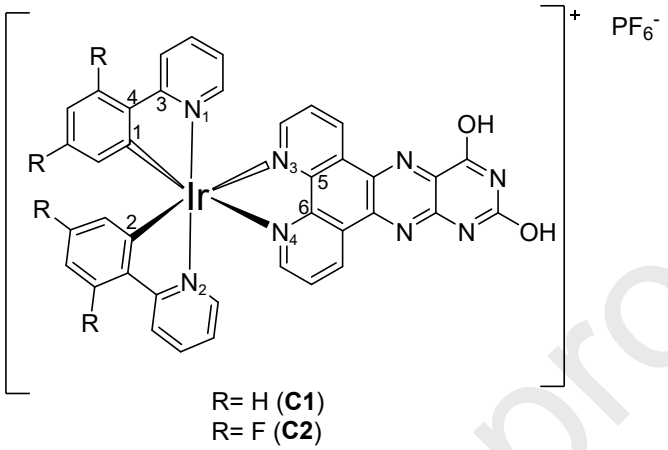

Fig. 1. Chemical structures of the cyclometalated Ir(III) complexes studied. Labeling atoms used to geometrical parameters (section 3.2)

2. Experimental Section

2.1. General remarks

Reagents and solvents were purchased from Sigma-Aldrich, with the exception of $IrCl_3$ hydrate, which was purchased from Precious Metals Online, PMO Pty LTD, Australia. All reactions were carried out under nitrogen atmosphere. All other chemicals were analytical grade reagents. All organic solvents used in this study were dried over appropriate drying agents. NMR spectra were recorded on an NMR Bruker Avance 400 instrument. Chemical shifts are given in parts per million relative to TMS [^{1}H, d($SiMe_4$) = 0]. For mass spectroscopy (MALDI-MS) measurements, the complex samples were prepared in a 3 mg/mL concentration in acetonitrile. The ppdh sample was prepared in a 3 mg/mL concentration in dimethyl sulfoxide. The spectra were obtained from mixtures of the samples with a matrix of α-cyano-4-hydroxycinnamic acid (CHCA, 10 mg/mL prepared with isopropyl alcohol) in a 1:1 ratio. An aliquot of 0.6 μL of these mixtures were placed in a carrier plate sample micro scout (Bruker Daltonics Inc., MA, USA). The acquisition of spectra was performed using MALDI-TOF Microflex equipment (Bruker Daltonics Inc., MA, USA) in positive and negative ion mode for complexes and positive ion mode for ppdh ligand, by reflection detection coupled with flexControl 3.0 program (Bruker Daltonik GmbH, Germany). The equipment was previously calibrated to obtain the spectra, with a standard external corresponding to a mixture of peptides of 1000-3000 Da. The final spectra correspond to a total of 15 scans of 30 laser impacts (450 laser impacts in total) randomly applied at different points of the samples. The spectrum analysis was performed using the flex-Analysis 2.2 program (Bruker Daltonik GmbH, Germany). The FT-IR spectra were recorded on a Bruker Vector-22 Spectrophotometer using KBr pellets. Cyclic voltammograms were obtained using a PalmSens 3 Instruments Potentiostat in a three-electrode cell configuration with a platinum disc working electrode of 0.02 cm^2 geometric area, a saturated Ag/AgCl reference electrode, and platinum wire counter electrode. All electrochemical measurements were carried out in anhydrous acetonitrile (ACN) solutions of Ir(III) complexes (1 mM) with 0.1 M $TBAPF_6$ as supporting electrolyte at a scan rate of 0.1 V s^{-1}. The UV-Vis spectra were registered using an Agilent

Technologies Cary 300 UV-Vis spectrophotometer. Photoluminescence spectra were taken on a Jasco Instrument spectrofluorometer. Solutions of the compounds were previously degassed with nitrogen for approximately 20 min. Emission quantum yields (Φ_{em}) were obtained with relative method using $[Ru(bpy)_3](PF_6)_2$ (Φ_{em} = 0.095 in acetonitrile [32]; Φ_{em} = 0.095 in dichloromethane [33]) as actinometers with degassed solutions. [34] [35] [36]. The 77 K luminescence measurements were performed by freezing alcoholic solutions (ethanol/methanol, 4/1) and taken on an Edinburg Instrument spectrofluorometer. Fluorescence lifetimes were measured using a time-correlated single-photon counting (TC-SPC) apparatus (PicoQuant Picoharp 300) equipped with a subnanosecond LED source (excitation at 380 nm) powered by a PicoQuant PDL 800-B variable (2.5−40 MHz) pulsed power supply. Time-resolved emission measurements in the ns-ms timescale were performed with a custom laser spectrometer composed of a Continuum Surelite II Nd:YAG laser (FWHM = 6–8 ns) with a frequency doubled, (532 nm, 330 mJ) or tripled, (355 nm, 160 mJ) option. Light emitted by the sample was focused onto the entrance slit of a 300 mm focal length Acton SpectraPro 2300i triple grating, flat field, double exit monochromator equipped with a photomultiplier detector (Hamamatsu R3896). Signals from the photomultiplier were processed by means of a Teledyne LeCroy 604Zi (400 MHz, 20 GS/s) digital oscilloscope.

Density Functional Theory (DFT) calculations were performed in the Gaussian16 [37] software package. From benchmark calculations, the PBE0[38] and M06-2X[39] functionals were selected to characterize the ground states and triplet excited states, respectively. The 6-31G(d,p) basis sets were adopted for H, C, N, O and F atoms [40]; the quasirelativistic pseudopotential and basis set LANL2DZ was used for Ir. [41] Singlet and triplet states of the complexes were fully optimized without geometry constraints, and vibrational frequencies were obtained to ensure that all the structures correspond to energy minima. Time-dependent DFT (TD-DFT) calculations were used to obtain the first 30 singlet and 6 triplet excited states; TD-DFT optimization at the M06-2X/6-31G(d,p)/LANL2DZ level was implemented to get the optimized structures of the emitting triplet excited states. Continuum solvent effects were included by the polarized continuum model (IEF-PCM)[42] using dichloromethane and acetonitrile as solvents.

2.2. General synthetic procedures

2.2.1 Ligand

The ppdh ligand was synthesized based on a previously reported procedure [31]. The precursor 5,6-diamino-2,4-dihydroxypyrimidine sulfate (1 eq.) was dissolved in hot water (70 mL), and the suspension was adjusted to pH 10 with NaOH until dissolved. Then, 1,10-phenanthroline-5,6-dione (1 eq.) dissolved in hot water (20 mL) was added. The mixture was stirred and refluxed for 17 hours, forming a yellow-brown precipitate which was filtered and washed subsequently with basic hot water, hot water, methanol, and acetone. The final product was isolated as a yellow solid in 60% yield (133 mg). FT IR: (KBr, ν/cm^{-1}): 3420 (O-H); 1628, 1590 (C=N); 1500, 1478 (C=C). ^1H NMR (400 MHz, CF_3CO_2D, 298 K): δ 10.30 (d, J = 8.00 Hz, H_3), 9.93 (d, J = 8.00 Hz, H_4), 9.42 (dd, J = 4.00 Hz/ 12.00 Hz, H_7 and H_8), 8.46 (dd, J = 4.00 Hz/ 12.00 Hz, H_5), 8.36 (dd, J = 4.00 Hz/ 12.00 Hz, H_6), MALDI-MS [$C_{16}H_8N_6O_2$], *m/z*: calc. 317.0782 and found 317.0781.

2.2.2 Complexes

Ir(III) dimers, ($[Ir(ppy)_2(\mu\text{-}Cl)]_2$ and $[Ir(F_2\text{-}ppy)_2(\mu\text{-}Cl)]_2$) were synthesized according to previous literature procedures [43] [44]. The Ir(III) complexes **C1** and **C2** were synthesized according to previous procedures with modifications. The ppdh ligand (2 eq.) and bimetallic precursor (1 eq.) were dissolved in ethylene glycol monomethyl ether (60 mL). The mixture was stirred and refluxed for 4 hours under a nitrogen atmosphere in darkness. Then, the mixture was cooled to room temperature, and 300 mL of a saturated aqueous solution of NH_4PF_6 were added until complete precipitation. The mixture was filtered and the solid was washed with water and hexane. The solid was recrystallized with dichloromethane and hexane.

[Ir(ppy)$_2$ppdh](PF$_6$) [C1]. The final product was isolated as a brown solid in 50% yield (80 mg). FT IR: (KBr, ν/cm^{-1}): 3407 (O-H); 3048(C-H)$_{arom}$; 1610 (C=N); 1570, 1471 (C=C); 840, 553 (P-F). ^{1}H NMR (400 MHz, DMSO-d$_6$, 298 K): δ 12.56 (s, H$_1$), 12.03 (s, H$_2$), 9.50 (d, *J* = 8.00, H$_3$), 9.42 (d, *J* = 8.00, H$_4$), 8.33 (d, *J* = 4.00 Hz, H$_7$), 8.27 (m, H$_8$, H$_9$, H$_{24}$, H$_5$, H$_6$), 7.92 (m, H$_{10}$, H$_{15}$, H$_{18}$, H$_{23}$), 7.60 (d, *J* = 4.00 Hz, H$_{12}$, H$_{21}$), 7.02 (m, H$_{11}$, H$_{22}$, H$_{14}$, H$_{19}$, H$_{16}$, H$_{17}$), 6.27 (d, *J* = 8.00 Hz, H$_{13}$, H$_{20}$). MALDI-MS, *m/z*: [Ir(ppy)$_2$ ppdh)]$_1$(PF$_6$)$_0$ calc. 817.1903 and found 817.1896; [Ir(ppy)$_2$ ppdh)]$_0$(PF$_6$)$_1$ calc. 144.9642 and found 144.5982.

[Ir(F$_2$ppy)$_2$ppdh](PF$_6$) [C2]. Isolated as an orange solid in 60% yield (118 mg). FT IR: (KBr, ν/cm^{-1}): 3394(O-H); 3081 (C-H)$_{arom}$; 1603 (C=N); 1575, 1480 (C=C); 831, 560 (P-F). ^{1}H NMR (400 MHz, DMSO-d$_6$, 298 K): δ/ppm= 12.59 (s, H$_1$), 12.07 (s, H$_2$), 9.54 (d, *J* = 8.00, H$_3$), 9.45 (d, *J* = 8.00, H$_4$), 8.44 (d, *J* = 8.00 Hz, H$_7$), 8.36 (d, *J* = 4 H$_8$), 8.31 (dd, *J* = H$_8$, H$_9$, H$_{24}$), 8.20 (m, H$_5$, H$_6$), 8.00 (t, *J* = 8.00 Hz, H$_{10}$, H$_{23}$), 7.66 (d, *J* = 8.00 Hz, H$_{12}$, H$_{21}$), 7.07 (m, H$_{11}$, H$_{22}$, H$_{16}$, H$_{17}$), 5.70 (d, *J* = 8.00 Hz, H$_{14}$, H$_{19}$). MALDI-MS, *m/z*: [Ir(F$_2$ppy)$_2$ppdh)]$_1$(PF$_6$)$_0$ calc. 889.1526 and found 889.1496; [Ir(F$_2$ppy)$_2$ppdh)]$_0$(PF$_6$)$_1$ calc. 144.9642 and found 144.5839.

For ^{1}H NMR characterization, each proton is labeled according to the chemical structures showed in the supporting information (S.I). For MALDI-MS characterization of the complexes, in the identification of positive and negative ion modes, the subscript 1 and 0 were assigned, according to the ionic fragment analyzed. MALDI-MS spectra are shown in the S.I.

3. Results and discussion

3.1. Synthesis and characterization

The ppdh ligand was prepared by a Schiff-base condensation between a 1,10-phenanthroline-5,6-dione and 5,6-diamino-2,4-dihydroxypyrimidine sulfate in basic medium and was isolated with yields larger than 60%. The FT-IR spectrum of the ligand is consistent with its molecular structure, observing its characteristic signals ν(C=N) = 1628 cm^{-1} and 1590 cm^{-1}, ν(C=C) = 1500 cm^{-1} and 1478 cm^{-1}, ν(O-H) ~ 3400 cm^{-1}. The ppdh ligand showed low solubility in most common solvents. Therefore, the ^{1}H NMR and COSY spectra were obtained in trifluoroacetic acid (Fig. S1 and S2 of SI), where the electronic barrier effect of the phenazine nitrogen is observed, which displaces H_3 and H_4 of phenanthroline moiety to a low field. However, the H_1 and H_2 signals of hydroxy groups of pteridino are not observed, which is attributed to overlap between these signals and the solvent signal. The spectrum was measured in DMSO (Fig. S3) to corroborate this effect, obtaining the spectrum in lower resolution, observing a signal at 10.5 ppm, which corresponds to H_1 and H_2. However, given the low resolution of the spectrum and in order to assign H_1 and H_2 with greater certainty, the spectrum of the ligand was measured in DMSO and deuterated water to generate a proton exchange, which corroborated the presence of alcohols in the ligand (Fig. S4).

The resulting complexes showed better solubility in common solvents compared with the free ligand. Therefore, the ^{1}H-NMR and COSY spectra were recorded in DMSO, observing that the main characteristics of the pattern observed in the free ligand spectrum remained. The coordination of the ppdh ligand with the metal is evidenced when comparing the spectrum of the free and coordinated ligand, where it is observed that the ligand protons shift to the high field in the complexes.

3.2. Geometrical Parameters

The geometrical parameters of the ground state (S_0) and lowest triplet state (T_1) (in dichloromethane as solvent) determined by theoretical calculations are shown in Table 1 (according to Fig. 1). A distorted octahedral geometry around the metal center is observed for both complexes. The S_0 structures of the two complexes present similar geometrical parameters; however, all the bond lengths are slightly more elongated for **C1** compared to **C2**, where the bonds involving the ancillary ligand (Ir-N3 and Ir-N4) undergo the highest variation. The electron-withdrawing character of the fluorine atom of complex **C2** produces an accumulation of electron density in the C^N ligand, so that, bond lengths are shortened. [45] Comparing the T_1 with respect to the S_0 structures, it was found that in both complexes the bond distances between Ir(III) and the cyclometalating ligands were shortened, while that bond lengths Ir-N3 and Ir-N4 (of the ancillary ligand) are more elongated in the excited state, where **C2** complex undergoes the largest variation (~0.06 Å), indicating a weakened interaction between metal and ancillary ligand. On the other hand, it was observed that O-H and C-O bond lengths presented similar characteristics in both complexes and that the addition of the -OH substituents on the ancillary ligand does not cause a significant change in the planarity of the phenazine fragment that contains it (see support information Table S1 and Fig. S14 of the SI). Concerning the bond angles, small variations were observed in the coordination centers that maintain a distorted octahedral geometry, as is typically observed in this type of complex. [46] [47]

Table 1. Selected bond lengths (Å), bond angles (º), and dihedral angles (º) of all complexes in the ground state (S_0) and first excited (T_1) states with dichloromethane as solvent.

Parameter	C1		C2	
	S_0	T_1	S_0	T_1
Bond length (Å)				
Ir-N1	2.083	2.075	2.054	2.072
Ir-N2	2.083	2.074	2.055	2.072
Ir-C1	2.021	1.990	2.002	1.988
Ir-C2	2.021	1.989	1.999	1.987
Ir-N3	2.221	2.240	2.166	2.229
Ir-N4	2.221	2.236	2.168	2.225
Bond angle (deg)				
C1-Ir-C2	89.83	89.20	89.10	88.99
C1-Ir-N1	80.08	80.58	80.41	80.68
C2-Ir-N2	80.08	80.57	80.51	80.69
N1-Ir-N2	173.87	174.34	173.88	174.20
C1-Ir-N3	97.54	97.85	97.65	97.98
C2-Ir-N3	172.27	172.81	172.03	172.80
N1-Ir-N3	88.06	87.26	87.82	87.85
N2-Ir-N3	97.17	97.28	97.03	96.82
N3-Ir-N4	75.19	74.73	76.62	75.11
C1-Ir-N4	172.26	172.20	173.93	172.84
Dihedral angle (deg)				
C1-C2-N4-N3	-3.80	-2.95	-2.90	-2.80
N1-C1-N2-N4	-8.46	-8.36	-7.34	-8.15
N1-N3-N2-C2	-8.00	-7.55	-7.60	-7.49

3.3. Frontier molecular orbital analysis

Fig. 2 shows the energy diagram and isosurfaces of the highest occupied molecular orbital (HOMO), lowest unoccupied molecular orbital (LUMO), and HOMO-LUMO energy gaps (ΔE_{HL}) calculated in dichloromethane. The contributions of molecular fragments to each molecular orbital (including energies) are listed in the Tables S2-S4 of the SI.

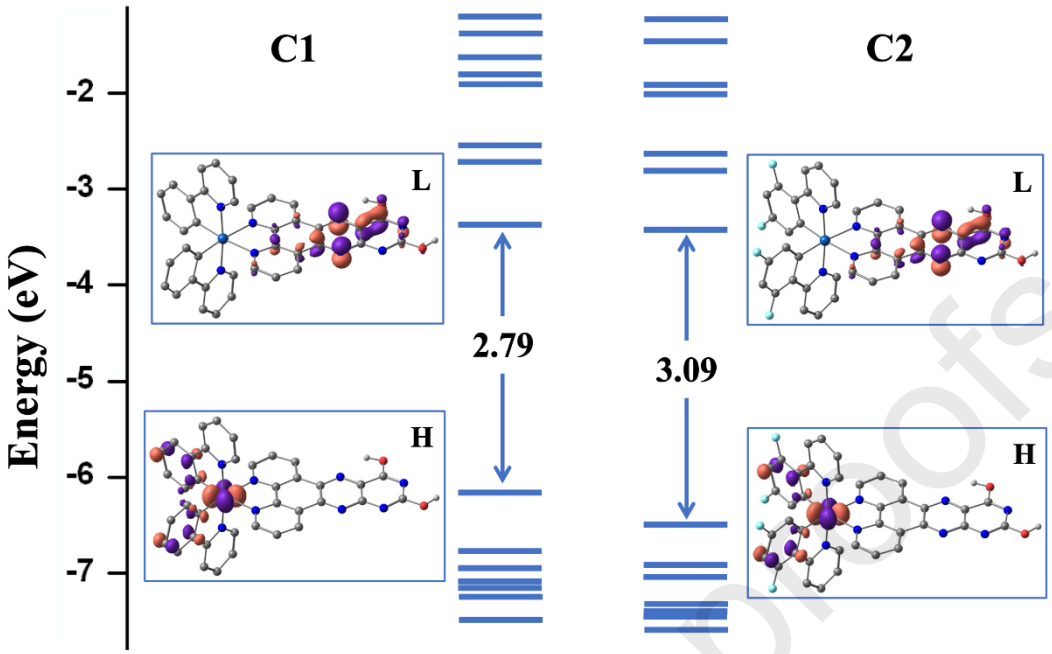

Fig. 2. Energy diagram and isosurfaces of molecular orbital of **C1** and **C2**. HOMO (H) and LUMO (L).

In both complexes, the LUMO level is at similar energies (~ -3.4 eV) as expected from the similar nature of the N^N ligands; while the HOMO is slightly stabilized in **C2** (-6.49 eV) compared to **C1** (-6.15 eV) due to the electron-withdrawing effects of the fluoride substituents on C^N ligand, accordingly, the ΔE_{HL} values are 2.79 eV and 3.09 eV for **C1** and **C2**, respectively. Regarding the composition of the frontier orbitals, it is noted that the HOMO density is mainly localized on Ir (~34%) and cyclometalating ligands (~62%) in both complexes; while, the HOMO-1 has a greater contribution from the cyclometalating ligand (92%) and some from Ir (6%). Note that the HOMO-1 is located at ~0.6 eV and ~0.4 eV below the HOMO in **C1** and **C2**, respectively. Meanwhile, HOMO-2 to HOMO-5 shows an increased contribution of up to 64% in the metal center. The HOMO-6 shows a mixed contribution by the ancillary ligand (up to 87%) and Ir (up to 22%). On the other hand, the LUMO density shows an extended π* character, which is fully localized on the phz moiety of the ancillary ligand, as in previous reports[48]. Likewise, LUMO+1 and LUMO+2 (0.6 eV above the LUMO) are also delocalized on the ancillary ligand, while LUMO+3 to LUMO+6 are mainly delocalized on the cyclometalating ligands (at least 71%).

Experimental insight into the position and energy of the frontier orbitals of the metal complexes **C1** and **C2** was attained by cyclic voltammetry (Table S5 of the SI). In both complexes, quasi-reversible redox processes are observed at positive potentials; according to the mixed contribution of the HOMO, the process is attributed to the Ir(IV)/(III) couple with some of the contribution from the cyclometalating ligands.[7b, 49] This process is observed at +1.40 V and +1.72 V for **C1** and **C2**, respectively, confirming the influence of the fluoride substituents into the stability of the HOMO level as noted above.[49-50] At negative potentials, reduction processes are associated with the ancillary ligand.[51] The first reduction process takes place at -1.17 V in both complexes following similar LUMO energy in both complexes. From the difference between the oxidation and the reduction potentials, $\Delta E_{ox\text{-}red}$ values of 2.57 and 2.89 V for **C1** and **C2**, respectively, can be calculated and observed to be qualitatively related to the trend in the HOMO-LUMO energy gap theoretically estimated (2.79 and 3.09 eV for **C1** and **C2**, respectively). In the same way, in the Fig. S15 of the Supporting Information HOMO-LUMO energy gap in acetonitrile as solvent follow the same trend (2.84 and 3.12 eV for **C1** and **C2,** respectively)

3.4. Absorption properties

The absorption spectra of the Ir(III) complexes in acetonitrile and dichloromethane solution at room temperature show similar characteristics (Table 2). The experimental spectra in dichloromethane are shown in Fig. 3, while those in acetonitrile are depicted in Fig. S16 of the SI. The absorption bands above 420 nm are attributable to metal-to-ligand charge-transfer (^{1}MLCT) and ligand-to-ligand change transfer (^{1}LLCT) transitions [50b, 52]; these bands are slightly blue-shifted in **C2** compared to **C1**, which is consistent with the stabilization of the HOMO in **C2** in the presence of the fluorinated cyclometalating ligands.[49, 53] In addition, contributions from spin-forbidden transitions to triplet states of charge transfer character might also be considered due to the high spin–orbit coupling of the Iridium metal. [52e, 54] Finally, the absorption bands observed in the UV region are assigned to spin-allowed ligand-centered (^{1}LC) $\pi \rightarrow \pi^*$ transitions, which involved both the ancillary and cyclometalating ligands.

Table 2. Photophysical and redox properties of Ir(III) complexes at room temperature under a nitrogen atmosphere.

Complex	λ_{abs}/nm		λ_{em}/nm			τ/μs [c]			Φ_{em}	
	ACN	DCM	ACN	DCM	77 K	ACN	DCM	77 K	ACN	DCM
C1	375 392 ~472	380 ~480	598	590	560	0.32	0.79	2.50	0.011	0.008
C2	370 388 ~450	375 393 ~472	530	533[a] 580[b]	482 519 559	1.16	0.33, 1.05	5.22, 6354	0.013	0.016

[a] excitation at 375 nm, [b] excitation at 393 nm, [c] excitation at 355 nm.

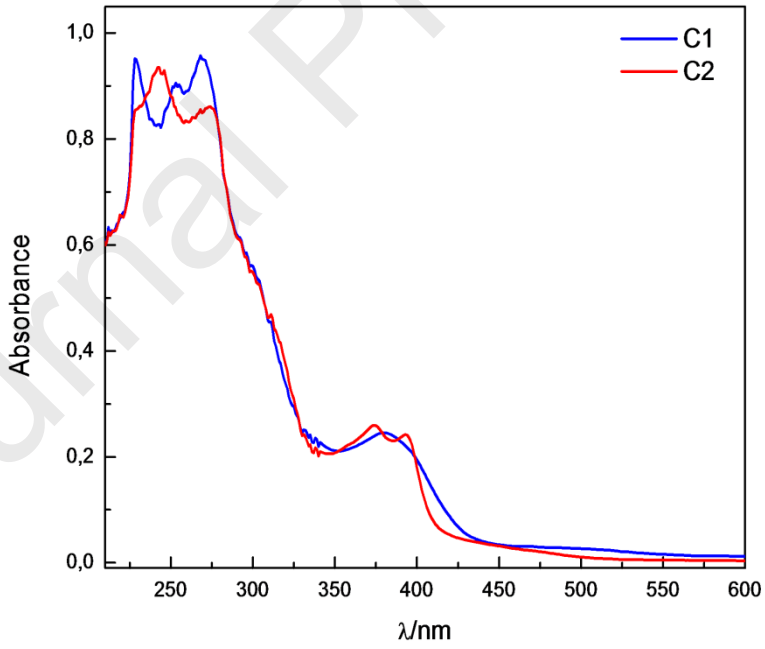

Fig. 3. UV-Visible absorption spectra of the Ir(III) complexes registered in dichloromethane solutions.

A detailed assignment of the absorption bands was then performed by TD-DFT calculations, where the results in dichloromethane are summarized in Table S6 of the SI. Fig. 4 shows the hole-electron distributions of the low-lying singlet excited states responsible for the absorption bands (in acetonitrile as solvent, singlet-singlet transitions and the hole-electron distributions of **C1** and **C2** as summary on Table S7 and Fig S17, respectively). In the case of complex **C1**, three singlet states (S_2, S_3, and S_4) are responsible for the broad experimental absorption at ~480 nm, which show electron promotion from the metal/phenyl moieties (C^N) to the ancillary ligand (mixed ^{1}MLCT/^{1}LLCT character): the S_2 state (at a computed wavelength of λ=476 nm) mainly involves HOMO→LUMO electron promotion; the S_3 state is due to HOMO→LUMO+2 (49%) and HOMO-1→LUMO (48%) electron transitions; the S_4 state mainly involves HOMO→LUMO+2 (49%) and HOMO-1→LUMO (45%) transitions. For the broad experimental band between 350-400 nm, TD-DFT calculation allows us to assign five allowed singlet excited states to be responsible: S_6, S_9, S_{11}, S_{14}, and S_{15}. The S_6 state (at λ=396 nm) mainly originates from HOMO-3→LUMO (76%) electron promotion, then with a mixed ^{1}MLCT/^{1}LLCT character. The S_9 state (at λ=375 nm) is mainly due to HOMO→LUMO+3 (96%) transition, where the electron promotion occurs from the metal/cyclometalating-ligand moieties toward the pyridine of cyclometalating-ligand, then with a mixed ^{1}MLCT/^{1}LC. The S_{11} state (at λ=368 nm) involves mainly HOMO-1→LUMO+1 (41%) and HOMO-5→LUMO (27%) transitions with mixed ^{1}MLCT/^{1}LLCT character. The S_{14} state (λ=358 nm) is the transition with the largest oscillator strength, and it mainly originates from HOMO-6→LUMO (79%) electron promotion; this state is characterized as ^{1}MLCT/^{1}LC, which mainly involves the phz fragment of the ancillary ligand in the ^{1}LC contribution. Finally, the S_{15} state (λ=345 nm) is due to HOMO-3→LUMO+1 (72%) electron transition (mixed ^{1}MLCT/^{1}LLCT character).

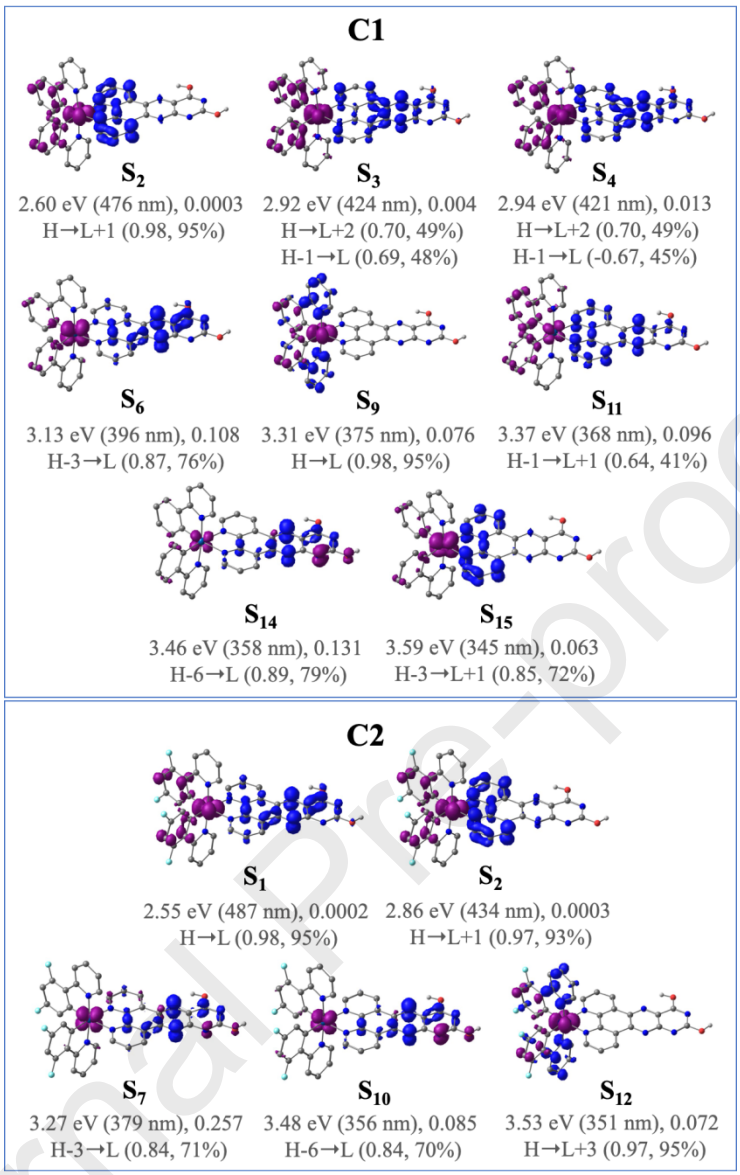

Fig. 4. Hole (purple) and electron (blue) distributions of selected singlet excited states (S_i) of **C1** and **C2**, including absorption energies (unit eV and nm) and oscillator strength (*f*); monoexcitations with weighting coefficients and percentage of contribution to the excited state wavefunction. Hydrogen atoms were deleted for clarity. Values are in dichloromethane as solvent.

In the case of complex **C2**, the experimental weak broad band at ~470 nm is assigned to transitions to the S_1 (λ=487 nm) and S_2 (λ=434 nm) states, which are poorly allowed (oscillator strength $f \approx 3 \cdot 10^{-4}$), and mainly involving HOMO→LUMO and HOMO→LUMO+1 electron transitions (mixed ^{1}MLCT/^{1}LLCT character), respectively. On the other hand, the S_7 state (at λ=379 nm) is assigned to the experimental absorption band at ~393 nm, which shows ^{1}MLCT character due to HOMO-3→LUMO electron transition. The experimental absorption band at ~375 nm is assigned to the S_{10} and S_{12} excited states. The S_{10} state (λ=356 nm) involves HOMO-6→LUMO (70%) electron transitions from the metal/phz moieties toward the fragment of the phz fragment of the N^N ligand (mixed ^{1}MLCT/^{1}LC character). Also, the S_{12} state (λ=351 nm) is mainly due to HOMO→LUMO+3 (95%) electron promotion with a mixed ^{1}MLCT/^{1}LLCT character.

It is worth pointing out that the absorption spectrum of the free ppdh ligand (Fig. S18 of the SI) shows intense bands at λ=263–340 nm, mainly due to π→π* transitions as expected for extended aromatic ligands. [26, 55] In addition, other transitions can be observed in the visible region (maximum at 446 nm), which can be assigned to intra-ligand charge transfer transitions (^{1}ILCT).[29] Interestingly, these ^{1}ILCT bands of the ppdh ligand completely disappear upon metal coordination, for instance, after the addition of Zn(II) cations (Fig. S16), leaving a structured absorption pattern with relative maxima at λ=369-387 nm that can be entirely assigned to spin-allowed of π→π* nature. With this in mind, the absorption bands around 350-420 nm in the experimental absorption spectrum of the Ir(III) complexes (see Fig. 3) can be directly assigned to ^{1}LC transitions centered in the ancillary ppdh ligand. In agreement with the experiments, TD-DFT calculation shows that ^{1}LC transitions centered in the ancillary ppdh ligand are main contributions in the S_{14} (λ=358 nm) and S_{10} state (λ=356 nm) of the **C1** and **C2** complexes, respectively. Consequently, excited states of LC character can take an active role in the excited state dynamics of complexes **C1** and **C2**, as is shown hereafter.

3.5. Luminescent properties

The emission spectra of the complexes were registered in both degassed acetonitrile and dichloromethane solutions as well as in a glassy matrix at 77 K and compared with the luminescence properties of the ppdh ligand in the presence of Zn(II) cations (Fig. S19). The photophysical parameters are in Table 2.

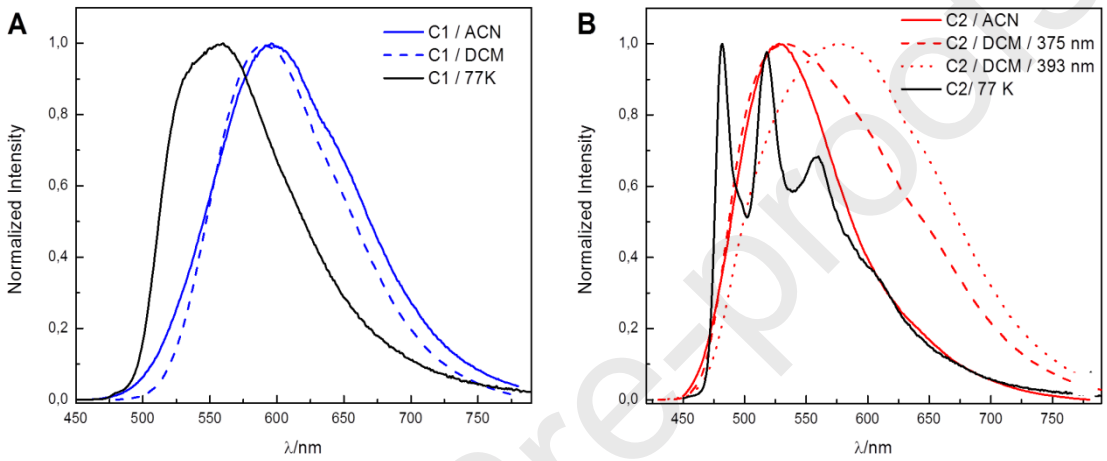

Fig. 5. Emission spectra of **A) C1** and **B) C2** in different conditions.

In acetonitrile at room temperature, the ppdh ligand (in the presence of Zn(II) ions) displays a structured emission band (Fig. S19) centered at 405 nm, which is attributable to ligand fluorescence (lifetime τ=0.55 ns, Fig. S20). In a glassy matrix at 77 K (4/1 EtOH/MeOH), beside the fluorescence, an intense phosphorescence is observed, which displays a structured profile with three relative maxima at 488, 521, and 554 nm (Fig. S19).The room temperature emission spectra of complexes **C1** and **C2** in acetonitrile and dichloromethane as well as those in a rigid matrix at 77 K are depicted in Fig. 5A and 5B, respectively. As expected, the luminescence of **C1** is red-shifted compared to that of **C2**, consistent with the stabilization of the occupied frontier orbitals in the latter due to the presence of fluoride substituents in the C^N ligand. The emission quantum yields are slightly larger in **C2** than **C1**, in agreement with energy-gap-law considerations and showed in table 2 [7a] [7b].

In the case of **C1**, the emission in dichloromethane (Fig. 5A) shows a maximum that is blue-shifted when compared to the value measured in acetonitrile (590 vs. 598 nm). This luminescence is attributable to phosphorescence of main MLCT/LLCT character and the spectral shift observed from CH_3CN to CH_2Cl_2 is in accordance with the energy destabilization of charge transfer emitting states in a less polar environment. [56] [57] In both cases, the shapes of the emission spectra are independent of the excitation wavelength with quantum yield is similar in both acetonitrile and dichloromethane (ca 1%) as solvent. Besides, the excited-state lifetime slightly increases from 0.32 to 0.79 μs on going from CH_3CN to CH_2Cl_2. At 77 K, complex **C1** displays a broad emission with a maximum at 560 nm (Fig. 5A). The blue shift observed with respect to acetonitrile and dichloromethane is attributable to the rigidochromic effect, which is typical of charge transfer emitting species. [58] The lifetime measured under these conditions (2.50 μs) is comparable to those of MLCT/LLCT emitters. [59] Overall, the photophysical behavior observed in **C1** is consistent with excited-state deactivation from a triplet metal-to-ligand or ligand-to-ligand charge-transfer (^{3}MLCT or ^{3}LLCT) excited states or a mixture of both, as has been described for related cationic Ir(III) complexes with similar ancillary ligands. [49, 60]. The ^{3}LC state localized on the ancillary ligand very likely lies at higher energy than the ^{3}MLCT/^{3}LLCT state. However, the weak emission quantum yields experimentally determined (ca 1%) can be possibly accounted for by a favorable participation of the ^{3}LC state within the excited state deactivation. Consistent with these considerations, theoretical calculations show that the radiative deactivation of the T_1 state displays a large contribution from a LUMO→HOMO-2 transition, involving π* and π orbitals of the phz moiety in the ancillary ligand (Fig. S21).

In the case of **C2**, the emission in acetonitrile solution displays a band centered at ca 530 nm, whose spectral profile is independent of the excitation wavelength. The lifetime measured by time-resolved emission amounts to 1.16 μs under oxygen-free conditions. Interestingly, different emission spectra were obtained in dichloromethane depending on the excitation wavelength (Fig. 5B). For instance, upon excitation at 375 nm (into the LC spin-allowed transition), the emission of complex **C2** displays a maximum at 533 nm, while by exciting at 393 nm into the MLCT band, the luminescence becomes much broader and shows a red-shifted maximum at 580 nm. This behavior thus suggests a more complex excited-

state dynamics in **C2** than in **C1**, particularly in CH_2Cl_2 as the solvent. To elucidate this issue, time-resolved emission spectra were recorded on complex **C2** in oxygen-free dichloromethane (Fig. 6). Upon excitation at 355 nm, the prompt spectrum detected (10 ns time delay) displays a broad profile with a maximum at ca 600 nm. This spectrum decreases in intensity within the subsequent 500 ns and shifts towards shorter wavelengths featuring a new maximum at ca 530 nm. The latter spectrum then decays within 5 µs. Interestingly, the time-resolved emission data in Fig. 6 can be well-modelled using two gaussian functions with maxima at ca 530 and 590 nm and FWHM of ca 70 and 130 nm, respectively (see Supporting Information, Fig. S22-S29), suggesting the presence of two different emitting states. Consistently, kinetic analysis of the emission decays yields two time-constants of 0.33 and 1.05 µs (average from different measurements), with the longer component being dominating at shorter wavelengths and thus assignable to the higher energy band and the shorter component ascribable to the ca 590 nm luminescence (Fig. S19 and S20). This experimental observation point towards a dual emission behavior of complex **C2** in CH_2Cl_2 as the solvent as observed for related iridium(III) complexes. [61] [62]

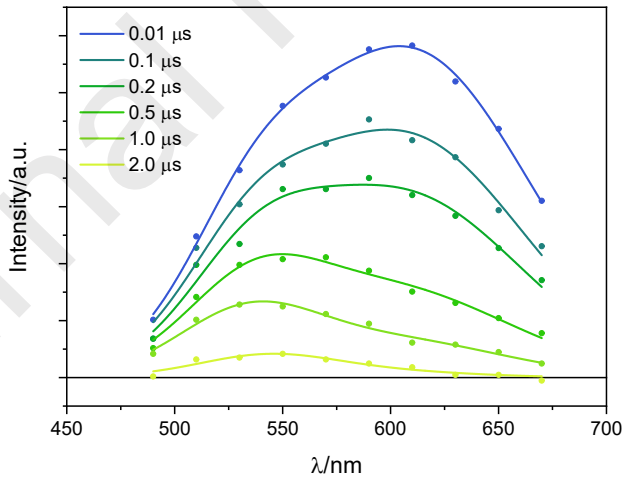

Fig. 6. Emission spectra of **C2** in dichloromethane at different time delays after excitation measured by laser flash photolysis (excitation at 355 nm).

Luminescence measurements at 77 K on **C2** (4/1 EtOH/MeOH glassy matrix) have been also performed to obtain additional insight and show an emission profile (Fig. 5B) with a vibrational progression, characteristic of the luminescence associate to a ligand-centered (LC) excited state. Interestingly, this spectrum closely matches the phosphorescence spectrum measured on the ppdh ligand in the presence of Zn(II) cations (Fig. S17). This observation suggests that in the rigid medium the ^{3}LC state localized on the ancillary ligand is responsible for the observed structured emission profile. This attribution is further confirmed by the detection of a long-lived (ms) component in the luminescence decay at 77 K, characteristic of ligand-based phosphorescence. [63]

Considering the results obtained by both steady-state and time-resolved emission analysis and taking into account the photophysical behavior of related iridium(III) complexes featuring dual emission behavior, [62] the photophysics of complex **C2** can be summarized as schematized in Fig. 7.

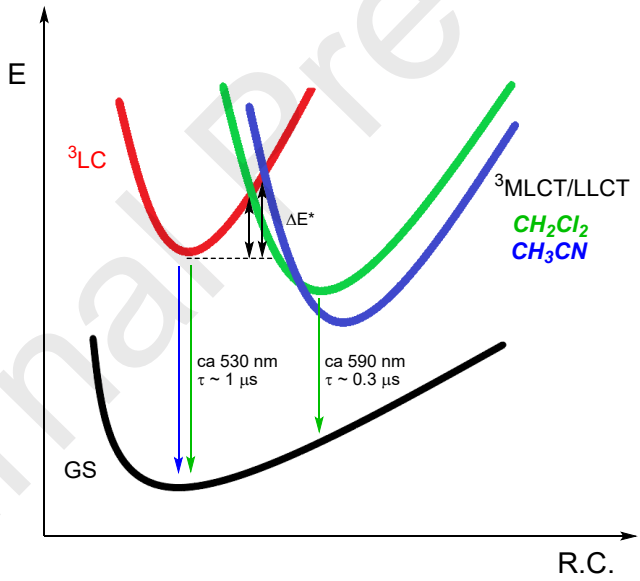

Fig. 7. Schematization of the potential energy surfaces of ground state and lowest excited states in complex **C2**: LC-based emission in CH_3CN (blue arrow) and dual emission in CH_2Cl_2 (green arrows).

The luminescence of complex **C2** in acetonitrile falls at comparable energy as the emission observed at 77 K thus suggesting that this emission can be confidently assigned to a radiative deactivation from an excited state of main ^{3}LC character. On the other hand, in dichloromethane a dual emission is observed with a red-shifted (faster) luminescence from a ^{3}MLCT/^{3}LLCT excited state and a blue-shifted (and slower) emission profile consistent with the ppdh-based ^{3}LC phosphorescence. The relevant contribution in the radiative deactivation in **C2** from an excited state of main LC character is also confirmed by TD-DFT calculations (Fig. S19). Overall, the photophysical behavior of complex **C2** can be explained considering the presence of an excited state of predominant ^{3}LC character and one of main ^{3}MLCT/^{3}LLCT nature at slightly lower energy with a non-negligible activation barrier between them (Fig. 7). [62]This activation energy may change as a function of the solvent used and is expected to be larger in the case of acetonitrile as the solvent than dichloromethane, considering the changes in both energy and nuclear geometry for excited states of CT nature. Accordingly, the observation of a predominant ^{3}LC emission in acetonitrile as the solvent is consistent with almost quantitative population of the ^{3}LC state upon light absorption and subsequent intersystem crossing and with the presence of a large activation barrier between the ^{3}LC and ^{3}MLCT/^{3}LLCT states leading to a negligible population, at room temperature, of the ^{3}MLCT/^{3}LLCT state. On the other hand, the dual emission in dichloromethane can be explained considering a smaller activation barrier between the triplet LC and CT states favoring population of the CT state from the triplet LC state (Fig. 7). The different emission shape observed by steady-state luminescence at different excitation wavelengths (Fig. 5B) might originate from an uneven population of either the ^{3}LC or the ^{3}MLCT/^{3}LLCT state from the corresponding singlet states, which, combined with the mutual activated population, may lead to potentially different fractions of triplet emitting states. Remarkably, the larger luminescence quantum yield observed in **C2** in dichloromethane than in acetonitrile (Table 2), in spite of the observed spectral red-shift and resulting energy-gap-law effects, very likely stems from the improved, positive contribution from the triplet excited state of charge transfer character.

Conclusion

The synthesis, structural characterization, and a deep analysis of the electronic properties of two Iridium complexes with the ancillary ligand pteridino[7,6-f][1,10]phenanthroline-1,13(10H,12H)-dihydroxy (ppdh) have been reported. The experimental results have also been complemented and corroborated by TD-DFT calculations. Both complexes show room temperature phosphorescence in both acetonitrile and dichloromethane solutions In **C1**, radiative deactivation occurs from a triplet excited state of predominant MLCT/LLCT nature. In **C2**, an excited state of triplet LC character localized on the ancillary ppdh ligand has a determining role in the excited state decay. Furthermore, in this latter case, the close vicinity of the ^{3}MLCT/^{3}LLCT and ^{3}LC states and the presence of an activation barrier between these excited states is responsible for a dual emissive behavior observed in dichloromethane as the solvent, as elucidated by both steady-state and time-resolved emission experiments. We believe that the detailed mechanistic analysis here presented may cast additional notions on the photophysical properties of iridium(III) complexes for the improved deployment of this class of metal complexes in diverse applications such as optoelectronic devices, sensors, imaging, and therapy.

Ackwnolegments

This work was financially supported by projects. I. González acknowledges FONDECYT N° 11180185 and CIP2018002; P. Dreyse acknowledges to PI_L_18_17 USM project and FONDECYT project N° 1201173; M Santander-Nelly acknowledges to FONDECYT project N° 3170663. D.C-A thanks the computational resources through the CONICYT/FONDEQUIP project EQM180180. Project supported by the Fund of Scientific and Technological Equipment, year 2018, code L318-04, Universidad Tecnológica Metropolitana. Powered@NLHPC: This research was partially supported by the supercomputing infrastructure of the NLHPC (ECM-02)."

References

[1] a) G. J. Meyer, *Inorganic chemistry* **2005**, *44*, 6852-6864; b) S. Ardo and G. J. Meyer, *Chemical Society Reviews* **2009**, *38*, 115-164.
[2] A. Sinopoli, C. J. Wood, E. A. Gibson and P. I. Elliott, *European Journal of Inorganic Chemistry* **2016**, *2016*, 2887-2890.
[3] K. Ocakoglu, E. Harputlu, P. Guloglu and S. Erten-Ela, *Synthetic metals* **2012**, *162*, 2125-2133.
[4] H. Yersin, A. F. Rausch, R. Czerwieniec, T. Hofbeck and T. Fischer, *Coordination Chemistry Reviews* **2011**, *255*, 2622-2652.
[5] P. Lima, F. Paz, C. Brites, W. Quirino, C. Legnani, M. C. e Silva, R. Ferreira, S. Júnior, O. Malta and M. Cremona, *Organic Electronics* **2014**, *15*, 798-808.
[6] M. M. Richter, *Chemical Reviews* **2004**, *104*, 3003-3036.
[7] a) I. González, P. Dreyse, D. Cortés-Arriagada, M. Sundararajan, C. Morgado, I. Brito, C. Roldán-Carmona, H. J. Bolink and B. Loeb, *Dalton Transactions* **2015**, *44*, 14771-14781; b) R. D. Costa, E. Orti, H. J. Bolink, F. Monti, G. Accorsi and N. Armaroli, *Angewandte Chemie International Edition* **2012**, *51*, 8178-8211.
[8] A. Zamora, G. Vigueras, V. Rodríguez, M. D. Santana and J. Ruiz, *Coordination Chemistry Reviews* **2018**, *360*, 34-76.
[9] A. D. Ostrowski and P. C. Ford, *Dalton Transactions* **2009**, 10660-10669.
[10] R. D. Rimmer, H. Richter and P. C. Ford, *Inorganic chemistry* **2009**, *49*, 1180-1185.
[11] G. Vitiello, A. Luchini, G. D'Errico, R. Santamaria, A. Capuozzo, C. Irace, D. Montesarchio and L. Paduano, *Journal of Materials Chemistry B* **2015**, *3*, 3011-3023.
[12] a) B. Yuan, J. Liu, R. Guan, C. Jin, L. Ji and H. Chao, *Dalton Transactions* **2019**, *48*, 6408-6415; b) J. S. Nam, M.-G. Kang, J. Kang, S.-Y. Park, S. J. C. Lee, H.-T. Kim, J. K. Seo, O.-H. Kwon, M. H. Lim and H.-W. Rhee, *Journal of the American Chemical Society* **2016**, *138*, 10968-10977.
[13] a) M. Valenzuela-Valderrama, V. Bustamante, N. Carrasco, I. A. González, P. Dreyse and C. E. Palavecino, *Photodiagnosis and Photodynamic Therapy* **2020**, 101662; b) M. Valenzuela-Valderrama, I. A. González and C. E. Palavecino, *Photodiagnosis and photodynamic therapy* **2019**.
[14] M. Luo, A. Liang, D. Liu, H. Wang, Z. Wang, Y. Chen and T. Cao, *Journal of Organometallic Chemistry* **2018**, *877*, 68-72.
[15] A. Reyna-Madrigal, N. Ortiz-Pastrana and M. A. Paz-Sandoval, *Journal of Organometallic Chemistry* **2019**, *886*, 13-26.
[16] C. Ge, X. Sang, W. Yao, L. Zhang and D. Wang, *Green Chemistry* **2018**, *20*, 1805-1812.
[17] K. P. S. Zanoni, R. L. Coppo, R. C. Amaral and N. Y. M. Iha, *Dalton Transactions* **2015**, *44*, 14559-14573.
[18] I. M. Dixon, J.-P. Collin, J.-P. Sauvage, L. Flamigni, S. Encinas and F. Barigelletti, *Chemical Society Reviews* **2000**, *29*, 385-391.
[19] N. J. Lundin, A. G. Blackman, K. C. Gordon and D. L. Officer, *Angewandte Chemie* **2006**, *118*, 2644-2646.

[20] C. G. Coates, L. Jacquet, J. J. McGarvey, S. E. Bell, A. H. Al-Obaidi and J. M. Kelly, *Journal of the American Chemical Society* **1997**, *119*, 7130-7136.
[21] D. Herebian and W. S. Sheldrick, *Journal of the Chemical Society, Dalton Transactions* **2002**, 966-974.
[22] A. Terenzi, G. Barone, A. Silvestri, A. M. Giuliani, A. Ruggirello and V. T. Liveri, *Journal of inorganic biochemistry* **2009**, *103*, 1-9.
[23] T. K. Schoch, J. L. Hubbard, C. R. Zoch, G.-B. Yi and M. Sørlie, *Inorganic chemistry* **1996**, *35*, 4383-4390.
[24] a) S. Stimpson, D. R. Jenkinson, A. Sadler, M. Latham, D. A. Wragg, A. J. Meijer and J. A. Thomas, *Angewandte Chemie International Edition* **2015**, *54*, 3000-3003; b) G. Li, L. Sun, L. Ji and H. Chao, *Dalton Transactions* **2016**, *45*, 13261-13276.
[25] M. Waterland, K. Gordon, J. McGarvey and P. Jayaweera, *Journal of the Chemical Society, Dalton Transactions* **1998**, 609-616.
[26] C. B. Larsen, H. van der Salm, C. A. Clark, A. B. Elliott, M. G. Fraser, R. Horvath, N. T. Lucas, X.-Z. Sun, M. W. George and K. C. Gordon, *Inorganic chemistry* **2014**, *53*, 1339-1354.
[27] C. Jia, S. X. Liu, C. Tanner, C. Leiggener, A. Neels, L. Sanguinet, E. Levillain, S. Leutwyler, A. Hauser and S. Decurtins, *Chemistry–A European Journal* **2007**, *13*, 3804-3812.
[28] C. Goze, C. Leiggener, S. X. Liu, L. Sanguinet, E. Levillain, A. Hauser and S. Decurtins, *ChemPhysChem* **2007**, *8*, 1504-1512.
[29] T. Ozawa, Y. Kishi, K. Miyamoto, Y. Wasada-Tsutsui, Y. Funahashi, K. Jitsukawa and H. Masuda, *Advanced Materials Research* **2006**, pp. 277-280.
[30] J.-G. Liu, B.-H. Ye, H. Chao, Q.-X. Zhen and L.-N. Ji, *Chemistry letters* **1999**, *28*, 1085-1086.
[31] F. Gao, H. Chao, F. Zhou, Y.-X. Yuan, B. Peng and L.-N. Ji, *Journal of inorganic biochemistry* **2006**, *100*, 1487-1494.
[32] H. Ishida, S. Tobita, Y. Hasegawa, R. Katoh and K. Nozaki, *Coordination chemistry reviews* **2010**, *254*, 2449-2458.
[33] J. V. Caspar and T. J. Meyer, *Journal of the American Chemical Society* **1983**, *105*, 5583-5590.
[34] S. Di Bella, C. Dragonetti, M. Pizzotti, D. Roberto, F. Tessore and R. Ugo in *Coordination and organometallic complexes as second-order nonlinear optical molecular materials*, Springer, **2010**, pp. 1-55.
[35] H. J. Bolink, E. Coronado, R. D. Costa, E. Ortí, M. Sessolo, S. Graber, K. Doyle, M. Neuburger, C. E. Housecroft and E. C. Constable, *Advanced Materials* **2008**, *20*, 3910-3913.
[36] C. Cebrián, M. Natali, D. Villa, M. Panigati, M. Mauro, G. D'Alfonso and L. De Cola, *Nanoscale* **2015**, *7*, 12000-12009.
[37] M. J. Frisch, G. W. Trucks, H. B. Schlegel, G. E. Scuseria, M. A. Robb, J. R. Cheeseman, G. Scalmani, V. Barone, G. A. Petersson, H. Nakatsuji, X. Li, M. Caricato, A. V. Marenich, J. Bloino, B. G. Janesko, R. Gomperts, B. Mennucci, H. P. Hratchian, J. V. Ortiz, A. F. Izmaylov, J. L. Sonnenberg, Williams, F. Ding, F. Lipparini, F. Egidi, J. Goings, B. Peng, A. Petrone, T. Henderson, D. Ranasinghe, V. G. Zakrzewski, J. Gao, N. Rega, G. Zheng, W. Liang, M. Hada, M. Ehara, K. Toyota, R. Fukuda, J. Hasegawa, M. Ishida, T. Nakajima, Y. Honda, O. Kitao,

H. Nakai, T. Vreven, K. Throssell, J. A. Montgomery Jr., J. E. Peralta, F. Ogliaro, M. J. Bearpark, J. J. Heyd, E. N. Brothers, K. N. Kudin, V. N. Staroverov, T. A. Keith, R. Kobayashi, J. Normand, K. Raghavachari, A. P. Rendell, J. C. Burant, S. S. Iyengar, J. Tomasi, M. Cossi, J. M. Millam, M. Klene, C. Adamo, R. Cammi, J. W. Ochterski, R. L. Martin, K. Morokuma, O. Farkas, J. B. Foresman and D. J. Fox in *Gaussian 16 Rev. B.01*, *Vol.* Wallingford, CT, **2016**.
[38] P. John and K. B. Perdew, *Phys. Rev. Lett* **1996**, *77*, 18.
[39] Y. Zhao and D. G. Truhlar, *Theoretical Chemistry Accounts* **2008**, *120*, 215-241.
[40] M. M. Francl, W. J. Pietro, W. J. Hehre, J. S. Binkley, M. S. Gordon, D. J. DeFrees and J. A. Pople, *The Journal of Chemical Physics* **1982**, *77*, 3654-3665.
[41] P. J. Hay and W. R. Wadt, *The Journal of Chemical Physics* **1985**, *82*, 299-310.
[42] B. Mennucci and J. Tomasi, *The Journal of chemical physics* **1997**, *106*, 5151-5158.
[43] M. S. Lowry and S. Bernhard, *Chemistry-A European Journal* **2006**, *12*, 7970-7977.
[44] K. K.-W. Lo, C.-K. Chung and N. Zhu, *Chemistry – A European Journal* **2006**, *12*, 1500-1512.
[45] M.-X. Song, G.-F. Wang, J. Wang, Y.-H. Wang, F.-Q. Bai and Z.-K. Qin, *Spectrochimica Acta Part A: Molecular and Biomolecular Spectroscopy* **2015**, *134*, 406-412.
[46] Q. Zhang, L. Wang, X. Wang, Y. Li and J. Zhang, *Organic Electronics* **2016**, *28*, 100-110.
[47] D. Han, L. Zhao, C. Pang and H. Zhao, *Polyhedron* **2017**, *126*, 134-141.
[48] J. A. Porras, I. N. Mills, W. J. Transue and S. Bernhard, *Journal of the American Chemical Society* **2016**, *138*, 9460-9472.
[49] I. González, D. Cortés-Arriagada, P. Dreyse, L. Sanhueza-Vega, I. Ledoux-Rak, D. Andrade, I. Brito, A. Toro-Labbé, M. Soto-Arriaza and S. Caramori, *European Journal of Inorganic Chemistry* **2015**, *2015*, 4946-4955.
[50] a) X. Li, B. Minaev, H. Ågren and H. Tian, *European Journal of Inorganic Chemistry* **2011**, *2011*, 2517-2524; b) A. B. Tamayo, S. Garon, T. Sajoto, P. I. Djurovich, I. M. Tsyba, R. Bau and M. E. Thompson, *Inorganic Chemistry* **2005**, *44*, 8723-8732.
[51] a) M. Martínez-Alonso, J. Cerdá, C. Momblona, A. Pertegás, J. M. Junquera-Hernández, A. Heras, A. M. Rodríguez, G. Espino, H. Bolink and E. Ortí, *Inorganic chemistry* **2017**, *56*, 10298-10310; b) D. Tordera, M. Delgado, E. Ortí, H. J. Bolink, J. Frey, M. K. Nazeeruddin and E. Baranoff, *Chemistry of Materials* **2012**, *24*, 1896-1903.
[52] a) S. Jo and Y. Choe, *Molecular Crystals and Liquid Crystals* **2017**, *654*, 221-233; b) H. C. Su, H. F. Chen, C. C. Wu and K. T. Wong, *Chemistry–An Asian Journal* **2008**, *3*, 1922-1928; c) H. C. Su, F. C. Fang, T. Y. Hwu, H. H. Hsieh, H. F. Chen, G. H. Lee, S. M. Peng, K. T. Wong and C. C. Wu, *Advanced Functional Materials* **2007**, *17*, 1019-1027; d) P. Dreyse, I. González, D. Cortés-Arriagada, O. Ramírez, I. Salas, A. González, A. Toro-Labbe and B. Loeb, *New Journal of Chemistry* **2016**, *40*, 6253-6263; e) J. E. Namanga, N. Gerlitzki, B. Mallick and A.-V. Mudring, *Journal of Materials Chemistry C* **2017**, *5*, 3049-3055.
[53] E. Baranoff, J.-H. Yum, M. Graetzel and M. K. Nazeeruddin, *Journal of Organometallic Chemistry* **2009**, *694*, 2661-2670.
[54] a) N. M. Shavaleev, R. Scopelliti, M. Grätzel, M. K. Nazeeruddin, A. Pertegás, C. Roldán-Carmona, D. Tordera and H. J. Bolink, *Journal of Materials Chemistry C* **2013**, *1*, 2241-2248; b) H. J. Bolink, L. Cappelli, S. Cheylan, E. Coronado, R. D. Costa, N. Lardiés, M. K. Nazeeruddin and E. Ortí, *Journal of Materials Chemistry* **2007**, *17*, 5032-5041; c)

R. n. D. Costa, F. Monti, G. Accorsi, A. Barbieri, H. J. Bolink, E. Ortí and N. Armaroli, *Inorganic chemistry* **2011**, *50*, 7229-7238.
[55] a) M. G. Fraser, A. G. Blackman, G. I. Irwin, C. P. Easton and K. C. Gordon, *Inorganic chemistry* **2010**, *49*, 5180-5189; b) E. Amouyal, A. Homsi, J.-C. Chambron and J.-P. Sauvage, *Journal of the Chemical Society, Dalton Transactions* **1990**, 1841-1845.
[56] Y. You and S. Y. Park, *Journal of the American Chemical Society* **2005**, *127*, 12438-12439.
[57] A. Beeby, S. Bettington, I. D. Samuel and Z. Wang, *Journal of Materials Chemistry* **2003**, *13*, 80-83.
[58] P. Chen and T. J. Meyer, *Chemical reviews* **1998**, *98*, 1439-1478.
[59] a) C. L. Ho, W. Y. Wong, Z. Q. Gao, C. H. Chen, K. W. Cheah, B. Yao, Z. Y. Xie, Q. Wang, D. G. Ma and L. X. Wang, *Advanced Functional Materials* **2008**, *18*, 319-331; b) P. Didier, I. Ortmans, A. Kirsch-De Mesmaeker and R. Watts, *Inorganic chemistry* **1993**, *32*, 5239-5245.
[60] I. González, M. Natali, A. R. Cabrera, B. Loeb, J. Maze and P. Dreyse, *New Journal of Chemistry* **2018**, *42*, 6644-6654.
[61] H. Benjamin, Y. Zheng, V. N. Kozhevnikov, J. S. Siddle, L. J. O'Driscoll, M. A. Fox, A. S. Batsanov, G. C. Griffiths, F. B. Dias and A. P. Monkman, *Dalton Transactions* **2020**, *49*, 2190-2208.
[62] S. Ladouceur, L. Donato, M. Romain, B. P. Mudraboyina, M. B. Johansen, J. A. Wisner and E. Zysman-Colman, *Dalton Transactions* **2013**, *42*, 8838-8847.
[63] M. T. Indelli, M. Ghirotti, A. Prodi, C. Chiorboli, F. Scandola, N. McClenaghan, F. Puntoriero and S. Campagna, *Inorganic chemistry* **2003**, *42*, 5489-5497.

Declaration of interests

☒ The authors declare that they have no known competing financial interests or personal relationships that could have appeared to influence the work reported in this paper.

☐The authors declare the following financial interests/personal relationships which may be considered as potential competing interests:

Two new iridium complexes were synthesized. The complex C2 shows an equilibration between the 3MLCT/3LLCT and 3LC states with luminescence indeed composed of two different patterns (533 and 580 nm) dependent on the excitation wavelength. The results add knowledge on the photophysical properties of iridium complexes for future applications.